NJC

PAPER

View Article Online
View Journal | View Issue

Cite this: *New J. Chem.*, 2017, **41**, 2255

Bi(III) immobilization inside MIL-101: enhanced photocatalytic performance†

Konstantin A. Kovalenko,*[ab] Natalia V. Ruban,[b] Sergey A. Adonin,[ab] Denis V. Korneev,[c] Simon B. Erenburg,[ad] Svetlana V. Trubina,[a] Kristina Kvashnina,[ef] Maxim N. Sokolov[ag] and Vladimir P. Fedin[ab]

Received 7th November 2016,
Accepted 30th January 2017

DOI: 10.1039/c6nj03482a

rsc.li/njc

A novel hybrid material Bi(III)@MIL-101 (Bi(III) = Bi-containing oxoclusters and MIL-101 = chromium(III) oxoterephthalate) was obtained by the intra-pore hydrolysis of guest bismuth(III) chloride in ammonia solution. This compound was characterized by chemical analysis, powder X-ray diffraction, nitrogen sorption and TEM techniques. According to the obtained data all Bi species are located only inside the matrix. The framework structure remains intact during all synthetic operations. The chemical nature of Bi(III)-containing clusters inside the MIL-101 matrix was suggested based on the EXAFS study. The catalytic activity of Bi(III)@MIL-101 in photodegradation of methyl red (MR) has been tested. The introduction of Bi(III)-species inside MIL-101 significantly increases the photocatalytic performance in comparison with layered BiOCl which was obtained under the same synthetic conditions without MIL-101.

Introduction

Over the last few years, the development of highly efficient photocatalytic materials has been representing one of the "hot topics" in modern chemistry. Among the possible application areas, treatment of industrial-use water containing organic pollutants is of special interest due to its great environmental importance.[1–7] In the great family of photoactive compounds which are commonly used (such as TiO_2, ZnO, CdS, *etc.*), bismuth oxohalides BiOX (X = Cl, Br, I) have been attracting much attention due to their high activity and tunability when used in hybrid materials.[8–18]

The main factors affecting the activity of the photocatalyst are the morphology, surface area and size of particles. These characteristics determine the goal of further development of synthetic methods and approaches which currently include solvothermal, microwave-assisted, ionic-liquid and many other routes.[19] The ultimate objectives are: (1) to achieve the largest surface area, (2) to maximize the stability of the catalyst morphology and (3) to find the simplest and cheapest method of synthesis. From this point of view, impregnation of photocatalyst nanoparticles into a stable porous matrix offers a suitable solution meeting at least two of these three targets. Perfect candidates for this role are metal–organic frameworks (MOFs).[20–29] This class of compounds has been successfully used for the immobilization of numerous types of catalysts, *e.g.* polyoxometalates[30–35] and metal nanoparticles,[36–40] resulting in a remarkable improvement of catalytic properties (activity, stability and recyclability) and/or changing homogeneous catalysis into heterogeneous. Also it is best known that MOFs possess their own photocatalytic activity.[2,41] Recently composites of BiOBr and two different MOFs, NH_2-MIL-125(Ti)[42] and UiO-66(Zr),[43] were prepared and their enhanced photocatalytic ability was demonstrated.

In this work we present an approach to inclusion compounds of the "Bi(III)@MOF" family. Mesoporous chromium(III) terephthalate $[Cr_3O(H_2O)_2(bdc)_3X]\cdot nH_2O$ (X = F^- or NO_3^-; H_2bdc = 1,4-benzenedicarboxylic acid; $n \approx 25$), commonly referred to as MIL-101, is one of the best known MOFs;[44] it was chosen for the experiments because of its outstanding stability in both acidic and weakly basic media. Inclusion of Bi(III) species into the stable MOF matrix results in a new photocatalytic system with enhanced activity in comparison with pure layered BiOCl. The photocatalytic properties were examined using a classical organic dye degradation process and methyl red was chosen as

[a] *Nikolaev Institute of Inorganic Chemistry SB RAS, 3 Akad. Lavrentiev Av., 630090 Novosibirsk, Russian Federation. E-mail: k.a.kovalenko@niic.nsc.ru; Fax: +7 (383) 330 9489; Tel: +7 (383) 330 9490*
[b] *Novosibirsk State University, 2 Pirogova Street, 630090 Novosibirsk, Russian Federation*
[c] *State Research Centre for Virology and Biotechnology "Vector", 630559 Koltsovo, Novosibirsk Region, Russian Federation*
[d] *Budker Institute of Nuclear Physics SB RAS, 11 Akad. Lavrentiev Av., 630090 Novosibirsk, Russian Federation*
[e] *European Synchrotron Radiation Facility, BP 220, 38043, Grenoble Cedex, France*
[f] *Helmholtz-Zentrum Dresden-Rossendorf (HZDR), Institute of Resource Ecology, P.O. Box 510119, 01314, Dresden, Germany*
[g] *Kazan Federal University, Alexander Butlerov Institute of Chemistry, Lobachevskogo Street 1/29, 420008, Kazan, Russian Federation*

† Electronic supplementary information (ESI) available: Further experimental data including PXRD, TEM, N_2 sorption, EXAFS spectra and catalytic tests. See DOI: 10.1039/c6nj03482a

a test pollutant because it is known as a potential carcinogenic azo dye. A special point was establishing Bi(III) particle structures inside MOF cavities.

Results and discussion

The introduction of Bi(III)-species was carried out by a standard hydrolysis technique of bismuth(III) chloride in ammonia solution. To avoid the formation of Bi(III) species outside the cages of the metal–organic framework, a two-step approach was used. In a typical experiment, MIL-101 was stirred with a hydrochloric acid solution of $BiCl_3$. After filtering off and drying at moderate temperature (*ca.* 50 °C) the solid sample was placed into ammonia solution with vigorous stirring to fix Bi(III) species inside MIL-101 cages. The resultant powder of Bi(III)@MIL-101 was filtered off again and dried in air at 60–70 °C.

Elemental analysis of Bi(III)@MIL-101 reveals that the Cr/Bi ratio is 33.4, which corresponds to 0.09 Bi atom per $[Cr_3O(bdc)_3]^+$ formula unit of MIL-101 or about 1 Bi atom per MIL mesocage on average. Interestingly, this ratio does not noticeably change when altering the time of impregnation.

To increase the Bi(III) content, the impregnation procedure was repeated several times. After the second impregnation the Cr/Bi ratio decreases down to 15.3. The third cycle additionally decreases the ratio down to 5.0, which corresponds to 0.6 Bi atom per formula unit or 6.8 per mesocage on average. The fourth and following impregnations do not alter the Bi content. Meanwhile, the chlorine content in the once impregnated sample is about 0.69 per $[Cr_3O(bdc)_3]^+$ formula unit, being higher than the Bi content. Therefore, it is impossible to assert stoichiometric bismuth oxochloride formation inside MIL-101 cages. On the other hand it is quite close to the number of tetrahedral microcages (0.5 per f.u.). As it was shown in our previous paper,[45] chloride-anions tend to occupy all such microcages thanks to fluoride-anion substitution. Therefore, chloride anions together with F^- and NO_3^- compensate the overall charge of the Bi(III)@MIL-101 material.

Transmission electron microscopy (TEM) confirms the absence of both discrete particles and any aggregates of BiOCl or other phases on the surface of MIL-101 crystals for the once impregnated sample. Moreover, it does not visualize any bulky particles of Bi(III) species in the crystals of MIL-101. This fact as well as identical chemical analysis in several nanoscale points has allowed us to assume that the distribution of Bi-containing particles in MIL-101 pores is rather uniform. However, twice and triple impregnated samples significantly differ from the once impregnated sample (Fig. 1): there are a lot of bulky particles on the MIL-101 crystal's surface. Therefore, we can conclude that the once impregnated sample is a true inclusion compound, whereas after second and third impregnation steps under our synthetic conditions a mixture of phases forms.

To confirm the crystallinity of the whole sample as well as its phase composition, the powder X-ray diffraction technique was used. PXRD patterns display the absence of peaks corresponding to layered BiOCl which can be obtained under the same

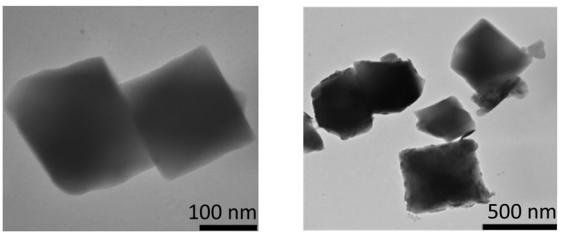

Fig. 1 TEM images of Bi(III)@MIL-101 after first (left) and third (right) impregnation.

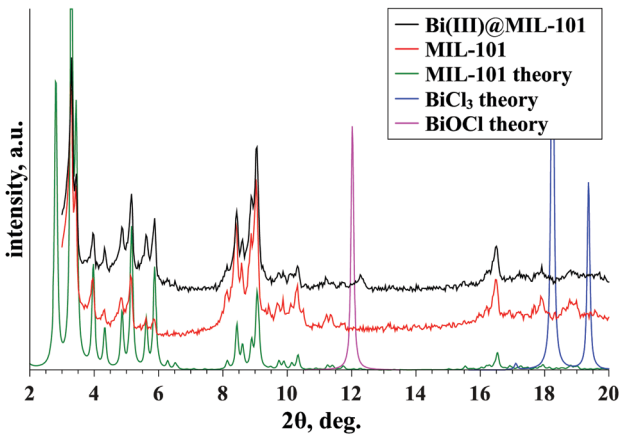

Fig. 2 XRPD patterns of Bi(III)@MIL-101 (black) and Cr-MIL-101 (red). Theoretical patterns of MIL-101 (green), $BiCl_3$ (blue) and layered BiOCl (pink) are given for comparison.

synthetic conditions without the MIL-101 matrix, initially $BiCl_3$ as well as any other phases. Instead, only peaks of MIL-101 were detected (Fig. 2). Slight changes in relative peak intensities (especially in the low angle range) are usually observed for inclusion compounds based on MOFs in general, and MIL-101 inclusion compounds in particular.[30,46] Thus, the MIL-101 structure is rigid and stable enough both for the procedure of Bi inclusion which proceeds in rather acidic solution (4 M HCl) and for hydrolysis of bismuth chloride in ammonia solution (pH ≈ 12).

Attempting to understand the structure of Bi(III)-species inside MIL-101, we have used high-energy-resolution X-ray absorption measurements (EXAFS-HERFD). The measured spectra, comparison of experimental and simulated spectra as well as parameters of the sample microstructure are given in the ESI† (Fig. S3–S5 and Table S2). According to these data, the coordination number of bismuth in Bi(III)@MIL-101 is 6 which is different from the bismuth coordination number in BiOCl where each Bi binds 4 oxygen and 4 chlorine atoms. Moreover, in spite of the quite big chlorine content in Bi(III)@MIL-101 (~0.7 per formula unit), there are no interactions between Bi and Cl atoms (Table S2, ESI†). Six coordination sites around each bismuth atom are distributed as follows: ~1 very short bond (2 Å), ~2 short bonds (2.5 Å), ~2 medium bonds (2.7 Å) and 1 long bond (2.9 Å). Analysis of interatomic distances performed for the crystal structures deposited in the Cambridge structural database (CSDB) reveals that the measured Bi–O distances found in

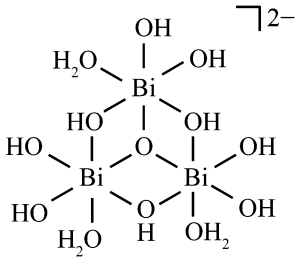

Fig. 3 Possible structure of Bi-oxoclusters inside MIL-101.

Bi(III)@MIL-101 could correspond to several coordination types summarized in Table S3 (ESI†). Taking into account that there are only two Bi atoms at a distance of 3.24 Å in the vicinity of Bi atoms, in addition to the six oxygen atoms, we could assume the predominant formation of trinuclear Bi clusters. The closest Bi–O distance is attributed to μ_3-O, two longer Bi–O distances belong to μ_2-OH or μ_2-OH_2, two other medium bonds may correspond to the terminal OH-ligand and the longest Bi–O distance to terminal aqua-ligands, respectively. The proposed structure of bismuth-oxo species is shown in Fig. 3. It must be noted that, according to the CSDB, there are more than 30 compounds containing such a type of substructural unit (the search was carried out without specifying the number of hydrogen atoms) but most of them are polynuclear clusters. To the best of our knowledge, the structures of the Bi oxocluster strongly depend on synthetic conditions and are very diverse. For example, Loye *et al.* reported the reactions of bismuth nitrate with terephthalic and nitroterephthalic acid under the same synthetic conditions resulting in different structure types containing the Bi_2O_2-layer and Bi_4O_3-chain motifs.[47] Oliver *et al.* have described synthesis, characterisation and some properties of hexa- and nonanuclear cationic clusters and have reported that the nature of sulfonic acid, reaction time, temperature and pH are crucial for controlling the dimensionality of cationic bismuth clusters.[48] Moreover such types of clusters are known for other metals but their structural characterisation is often very difficult due to their high lability. Thus, Leung *et al.* have reported the crystallisation of the hydroxobridged Zr(IV) complexes with Kläui's tripodal ligand.[49] Thuéry have used the supramolecular approach by adding cucurbit[6]uril for crystallization of trinuclear clusters with uranyl moieties.[50] It means that the unique surrounding of MIL-101 mesocages may result in the formation and stabilisation of unusual and still structurally unknown Bi clusters. It means that the structure of Bi-containing particles formed in the presence and in the absence of MIL-101 is absolutely different and therefore their catalytic activity should have significant differences too.

Nitrogen sorption isotherms of both Cr-MIL-101 and Bi(III)@MIL-101 have the same shape, which corresponds to mesoporous MOFs (Fig. S6, ESI†). The principle textural properties of initial MIL-101 and Bi(III)@MIL-101 are summarized in Table 1. Pore volumes obtained for MIL-101 and Bi(III)@MIL-101 are 1.89 and 1.02 mL g^{-1}, respectively. Contemporaneously the BET surface area decreases from 3863 m^2 g^{-1} for MIL-101 to 2065 m^2 g^{-1} for Bi(III)@MIL-101. These facts clearly indicate

Table 1 Parameters of the pore structure for MIL-101 and Bi(III)@MIL-101

Compound	Specific surface area/m^2 g^{-1}		V_{pore}/ cm^3 g^{-1}	V_{ads} (N_2)/ cm^3 (STP) g^{-1}
	Langmuir	BET		
MIL-101	5762	3863	1.89	1226
Bi(III)@MIL-101	2926	2065	1.02	653

that Bi particles occupy some space inside the mesocages of MIL-101, although they are still accessible and not blocked by these particles. On the other hand, the micropore volume significantly decreased for Bi(III)@MIL-101 (see the pore size distribution and cumulative volume curve in Fig. S7, ESI† for details); that displays the blocking of microcages of the MIL structure after the introduction of Bi-containing particles. Taking into account the absence of Bi–Cl interaction found from EXAFS data, significant changes of pore size distribution in MIL-101 and Bi(III)@MIL-101 could be explained by filling of tetrahedral microcages of the framework by chlorine anions whereas Bi(III) containing particles are located in mesocages. The same phenomenon of chlorine distribution into the smaller cavities was established for MIL-101 treated with sodium chloride solution from direct calorimetric experiments which are described in our previous paper.[45]

To investigate the catalytic activity of Bi(III)@MIL-101, photodegradation of methyl red (MR) has been chosen as a test reaction. The full decolorization of MR solution (3.5×10^{-5} M) was observed in 50–60 min under mercury lamp irradiation. The initial rate constant is quite high ($k = 0.037 \pm 0.005$ min^{-1} and $\tau_{1/2}$ = 18 min 44 s). The process is first-order over the first minutes; consequent changes of kinetics may be related to further oxidation and decomposition of MR primary degradation products (Fig. 4). It should be noted that pure MIL-101 is not active in MR degradation during the studied period of time and MR is stable under UV-light irradiation during this period (Table S3, ESI†).

XRPD and elemental analysis of the sample after the catalytic experiment display that Bi(III)@MIL-101 preserves both

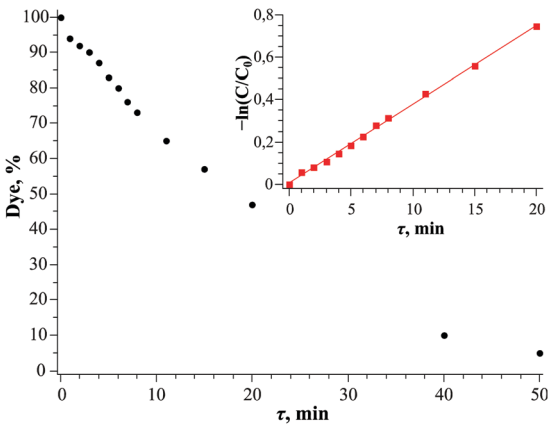

Fig. 4 Kinetics of methyl red degradation in the presence of Bi(III)@MIL-101 under mercury lamp irradiation. The linearisation in first-order coordinates is shown in inset.

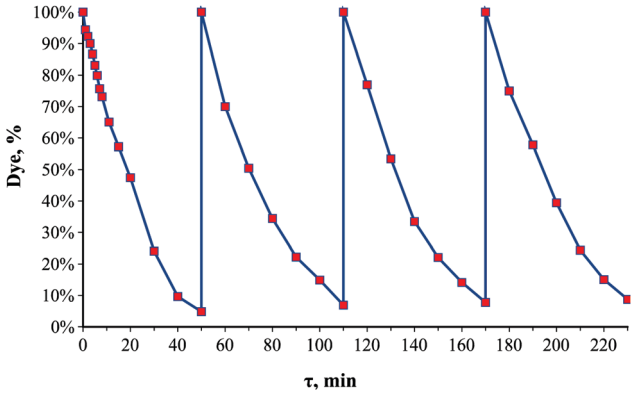

Fig. 5 Catalytic cycles of MR degradation in the presence of Bi(III)@MIL-101 under mercury lamp irradiation.

composition and crystallinity (Fig. S2 and Table S1, ESI†). The reaction solution was tested upon leaching of Bi species using atomic absorption spectroscopy. As a result, Bi concentration was found to be below the detection limit of this method (0.5 μg mL^{-1}) which means that leaching is less than 0.5% (if any). Therefore, we could conclude that the catalytic process has a truly heterogeneous nature.

To check if the activity of Bi(III)@MIL-101 changes in the case when the substrate is added to the solution continually (and the products of MR decomposition are accumulated in solution), the "portionwise addition" experiment was conducted (see the ESI† for a detailed description). It reveals that Bi(III)@MIL-101 preserves immutable activity after at least four catalytic cycles (Fig. 5), significantly exceeding those for pure BiOCl. The full decolorization of methyl red solution is observed in 20 min (see Fig. S9, ESI†) when using 10 mg of BiOCl (8 mg of Bi) or in a maximum of 60 min when using 15 mg of Bi(III)@MIL-101 containing *ca.* 0.4 mg of Bi. So the specific activity of the Bi(III)@MIL-101 catalyst is 20/60 × 8/0.4 = 6.7 times higher than that of pure BiOCl. While pure MIL-101 did not reveal any photocatalytic activity at all (Table S3, ESI†), the enhancement behaviour of Bi(III)@MIL-101 occurred due to the stabilization of small oxo-hydroxo Bi(III) clusters immobilized in the cavities of MOFs.

Experimental section

General remarks

All chemicals and solvents were at least of analytical grade and were used as purchased without additional purification. PXRD data were obtained on a Shimadzu XRD 7000S diffractometer with λ Cu ($K\alpha_1$, $K\alpha_2$) = 1.54059, 1.54439. Elemental analysis of Cr, Bi and Cl was carried out by X-ray fluorescence spectroscopy in several nanoscale points for controlling sample uniformity using a Bruker MISTRAL M1 apparatus. An analysis of the porous structure was performed by a nitrogen cryoadsorption technique using an automated gas sorption analyzer Autosorb iQ (Quantachrome Instruments) at 77 K. The samples were preliminarily degassed in a vacuum at 450 K for 12 hours. N_2 adsorption–desorption isotherms were measured within the range of relative pressures of 10^{-4} to 0.99. The specific surface area was calculated from the data obtained on the basis of the conventional BET and Langmuir models. The total pore volume was estimated from nitrogen uptake at P/P_0 = 0.95. The standard Saito & Foley approach, as the most appropriate for the studied materials, was employed to estimate the pore size distribution. Images of the samples were obtained by transmission electron microscopy using a JEM 1400 instrument (Jeol, Japan) at 120 kV with standard sample preparation.

Synthesis of compounds

Synthesis of Cr-MIL-101. The crystalline Cr-MIL-101 product was hydrothermally synthesized at 220 °C for 6 h from the mixture of $Cr(NO_3)_3{\cdot}9H_2O$ (1.2 g, 3 mmol), terephthalic acid (0.5 g, 3 mmol), 1 mL of 3 M HF (3 mmol) and 15 mL of water. Then the autoclave reactor was cooled to room temperature for 3 h to obtain larger crystals of the unreacted terephthalic acid which were removed by filtration using a glass filter with a pore size between 40 and 100 μm. Finally the as-synthesized solid was filtered off using paper filter. The purification procedure included two steps: double solvothermal treatment with DMF (50 mL of DMF per 1 g of MIL-101) at 60 °C for 2 h and then double treatment with EtOH at 75 °C for 2 h in the same MIL-101 : solvent ratio. The resulting material was dried overnight at 80 °C under an air atmosphere.

Synthesis of Bi(III)@MIL-101. In a typical experiment 200 mg of MIL-101 was added to 2 mL solution of $BiCl_3$ (20 mg) in 4 M HCl. After 30 min of stirring at room temperature the green solid was filtered off and dried at 70 °C in air. After that the dry sample was put into 10% ammonia solution (21 mL). After 15 min of stirring the solid of Bi(III)@MIL-101 was filtered off and dried at 70 °C in air again. Yield: 210 mg.

Synthesis of BiOCl. $BiCl_3$ (100 mg) was dissolved in 10 mL of 1 M HCl solution. After that 20 mL of aqueous ammonia (1 : 2) was added to the solution under vigorous stirring. The white solid obtained was filtered off, and washed with water, ethyl alcohol and acetone. Yield: 37 mg.

EXAFS-HERFD

High-energy-resolution X-ray absorption measurements were performed at the beamline ID26 of the European Synchrotron Radiation Facility. The electron energy was 6.0 GeV, and the ring electron current was varied between 180 and 200 mA. The energy of the X-ray incident beam was selected using the reflection from a double Si[111] crystal monochromator. Rejection of higher harmonics was achieved by two Si mirrors with Pd and Cr layers located at 2.5 mrad angle relative to the incident beam. The energy calibration was performed using a Bi metal sample. High-energy-resolution fluorescence detection (HERFD) spectra were measured with an X-ray emission spectrometer at 12 K. The Bi HERFD spectra at the L3-edge were obtained by recording the intensity of the Bi $L\alpha_1$ emission line (10 839 eV) as a function of the incident energy. The emission energy was selected using the ⟨660⟩ reflection of four spherically bent Ge crystal analyzers (with R = 1 m). Each Bi HERFD-XANES scan was collected in 30 s with a step size of 0.1 eV and usually used averaging of 10–20 scans.

Full Bi EXAFS-HERFD spectra over a 1000 eV range were measured in 180 s with a step size of 0.2 eV and averaging of 5 scans.

Catalytic tests

In a typical experiment, 10–20 mg of catalyst (pure MIL-101, Bi(III)@MIL-101 or pure BiOCl) was heated at 100 °C until the weight loss stopped and then was put into 10 mL solution of methyl red (3.7×10^{-5} M, 10 mg L^{-1}). The mixture was irradiated by a mercury lamp (1 kW) at room temperature (25–27 °C). The methyl red concentration was checked by UV-Vis spectroscopy ($\lambda \approx 500$ nm) with the addition of 0.1 M HCl solution for pH adjustment.

Conclusions

To conclude, the hybrid photocatalyst – Bi(III) impregnated in the metal–organic framework matrix – has been obtained and tested, displaying an outstanding activity which exceeds that of pure layered BiOCl prepared under similar synthetic conditions. The material Bi(III)@MIL-101 obtained is stable and active at least in four catalytic cycles, and demonstrates the truly heterogeneous nature of catalysis in azo dye photodegradation. According to the EXAFS study the structure of oxo-hydroxo Bi(III) clusters inside MIL-101 cages was assumed. Interestingly, such a structure type is known but not very common for Bi compounds. These results allow us to propose that this strategy can be successfully expanded further (1) to other Bi(III) oxohalides and (2) to other MOFs with different porosities, controlling the size of Bi(III) polynuclear clusters and access of various organic substrates. This will yield a new family of highly active photocatalysts suitable for environmental applications.

Acknowledgements

This work was supported by the Russian Science Foundation (Grant No. 14-23-00013).

Notes and references

1 S. Dong, J. Feng, M. Fan, Y. Pi, L. Hu, X. Han, M. Liu, J. Sun and J. Sun, *RSC Adv.*, 2015, **5**, 14610.
2 C. C. Wang, J. R. Li, X. L. Lv, Y. Q. Zhang and G. S. Guo, *Energy Environ. Sci.*, 2014, **7**, 2831.
3 G. Aragay, F. Pino and A. Merkoçi, *Chem. Rev.*, 2012, **112**, 5317.
4 R. K. Upadhyay, N. Soin and S. S. Roy, *RSC Adv.*, 2014, **4**, 3823.
5 M. R. Hoffmann, S. T. Martin, W. Choi and D. W. Bahnemann, *Chem. Rev.*, 1995, **95**, 69.
6 A. Di Paola, E. García-López, G. Marcì and L. Palmisano, *J. Hazard. Mater.*, 2012, **211–212**, 3.
7 J. Xiao, Y. Xie and H. Cao, *Chemosphere*, 2015, **121**, 1.
8 S. Weng, Z. Pei, Z. Zheng, J. Hu and P. Liu, *ACS Appl. Mater. Interfaces*, 2013, **5**, 12380.
9 A. Biswas, R. Das, C. Dey, R. Banerjee and P. Poddar, *Cryst. Growth Des.*, 2014, **14**, 236.
10 X. Zhang, X. B. Wang, L. W. Wang, W. K. Wang, L. L. Long, W. W. Li and H. Q. Yu, *ACS Appl. Mater. Interfaces*, 2014, **6**, 7766.
11 W. Zhang, Q. Zhang and F. Dong, *Ind. Eng. Chem. Res.*, 2013, **52**, 6740.
12 F. Tian, Y. Zhang, G. Li, Y. Liu and R. Chen, *New J. Chem.*, 2015, **39**, 1274.
13 X. Liu, H. Yang, H. Dai, X. Mao and Z. Liang, *Green Chem.*, 2014, **17**, 199.
14 F. Shen, L. Zhou, J. Shi, M. Xing and J. Zhang, *RSC Adv.*, 2015, **5**, 4918.
15 W. Yang, Y. Wen, D. Zeng, Q. Wang, R. Chen, W. Wang and B. Shan, *J. Mater. Chem. A*, 2014, **2**, 20770.
16 Y. Zuo, C. Wang, Y. Sun and J. Cheng, *Mater. Lett.*, 2015, **139**, 149.
17 J. Hu, W. Fan, W. Ye, C. Huang and X. Qiu, *Appl. Catal., B*, 2014, **158–159**, 182.
18 L. Lei, H. Jin, Q. Zhang, J. Xu, D. Gao and Z. Fu, *Dalton Trans.*, 2015, **44**, 795.
19 L. Ye, Y. Su, X. Jin, H. Xie and C. Zhang, *Environ. Sci.: Nano*, 2014, **1**, 90.
20 L. Ma, C. Abney and W. Lin, *Chem. Soc. Rev.*, 2009, **38**, 1248.
21 M. O'Keeffe, *Chem. Soc. Rev.*, 2009, **38**, 1215.
22 A. U. Czaja, N. Trukhan and U. Müller, *Chem. Soc. Rev.*, 2009, **38**, 1284.
23 Z. Wang and S. M. Cohen, *Chem. Soc. Rev.*, 2009, **38**, 1315.
24 J. Lee, O. K. Farha, J. Roberts, K. A. Scheidt, S. T. Nguyen and J. T. Hupp, *Chem. Soc. Rev.*, 2009, **38**, 1450.
25 N. Stock and S. Biswas, *Chem. Rev.*, 2012, **112**, 933–969.
26 S. M. Cohen, *Chem. Rev.*, 2012, **112**, 970–1000.
27 L. E. Kreno, K. Leong, O. K. Farha, M. Allendorf, R. P. Van Duyne and J. T. Hupp, *Chem. Rev.*, 2012, **112**, 1105–1125.
28 M. Yoon, R. Srirambalaji and K. Kim, *Chem. Rev.*, 2012, **112**, 1196–1231.
29 P. Horcajada, R. Gref, T. Baati, P. K. Allan, G. Maurin, P. Couvreur, G. Férey, R. E. Morris and C. Serre, *Chem. Rev.*, 2012, **112**, 1232–1268.
30 N. V Maksimchuk, K. A. Kovalenko, S. S. Arzumanov, Y. A. Chesalov, M. S. Melgunov, A. G. Stepanov, V. P. Fedin and O. A. Kholdeeva, *Inorg. Chem.*, 2010, **49**, 2920–2930.
31 N. V Maksimchuk, O. A. Kholdeeva, K. A. Kovalenko and V. P. Fedin, *Isr. J. Chem.*, 2011, **51**, 281–289.
32 W. Salomon, F.-J. Yazigi, C. Roch-Marchal, P. Mialane, P. Horcajada, C. Serre, M. Haouas, F. Taulelle and A. Dolbecq, *Dalton Trans.*, 2014, **43**, 12698.
33 C. M. Granadeiro, A. D. S. Barbosa, S. Ribeiro, I. C. M. S. Santos, B. de Castro, L. Cunha-Silva and S. S. Balula, *Catal. Sci. Technol.*, 2014, **4**, 1416–1425.
34 L. H. Wee, F. Bonino, C. Lamberti, S. Bordiga and J. A. Martens, *Green Chem.*, 2014, **16**, 1351–1357.
35 C. M. Granadeiro, P. Silva, V. K. Saini, F. A. A. Paz, J. Pires, L. Cunha-Silva and S. S. Balula, *Catal. Today*, 2013, **218–219**, 35–42.

36 J. Hermannsdörfer and R. Kempe, *Chem. – Eur. J.*, 2011, **17**, 8071–8077.
37 N. Cao, L. Yang, H. Dai, T. Liu, J. Su, X. Wu, W. Luo and G. Cheng, *Inorg. Chem.*, 2014, **53**, 10122–10128.
38 Y. Huang, Z. Lin and R. Cao, *Chem. – Eur. J.*, 2011, **17**, 12706–12712.
39 Y. Pan, B. Yuan, Y. Li and D. He, *Chem. Commun.*, 2010, **46**, 2280.
40 X. Li, Z. Guo, C. Xiao, T. W. Goh, D. Tesfagaber and W. Huang, *ACS Catal.*, 2014, **4**, 3490–3497.
41 A. Dhakshinamoorthy, A. M. Asiri and H. García, *Angew. Chem., Int. Ed.*, 2016, **55**, 5414–5445.
42 S.-R. Zhu, P.-F. Liu, M.-K. Wu, W.-N. Zhao, G.-C. Li, K. Tao, F.-Y. Yi and L. Han, *Dalton Trans.*, 2016, **45**, 17521–17529.
43 Z. Sha and J. Wu, *RSC Adv.*, 2015, **5**, 39592–39600.
44 G. Ferey, C. Mellot-Draznieks, C. Serre, F. Millange, J. Dutour, S. Surble and I. Margiolaki, *Science*, 2005, **309**, 2040–2042.
45 E. A. Berdonosova, K. A. Kovalenko, E. V Polyakova, S. N. Klyamkin and V. P. Fedin, *J. Phys. Chem. C*, 2015, **119**, 13098–13104.
46 V. G. Ponomareva, K. A. Kovalenko, A. P. Chupakhin, D. N. Dybtsev, E. S. Shutova and V. P. Fedin, *J. Am. Chem. Soc.*, 2012, **134**, 15640–15643.
47 A. C. Wibowo, M. D. Smith and H.-C. zur Loye, *CrystEngComm*, 2011, **13**, 426–429.
48 D. L. Rogow, H. Fei, D. P. Brennan, M. Ikehata, P. Y. Zavalij, A. G. Oliver and S. R. J. Oliver, *Inorg. Chem.*, 2010, **49**, 5619–5624.
49 X.-Y. Yi, Q.-F. Zhang, T. C. H. Lam, E. Y. Y. Chan, I. D. Williams and W.-H. Leung, *Inorg. Chem.*, 2006, **45**, 328–335.
50 P. Thuéry, *Cryst. Growth Des.*, 2011, **11**, 3282–3294.

